Efficient Spectrofluorimetric Analysis of Single-Walled Carbon Nanotube Samples

John-David R. Rocha,[†,‡] Sergei M. Bachilo,[†] Saunab Ghosh,[†] Sivaram Arepalli,[§] and R. Bruce Weisman[*,†]

[†]Department of Chemistry and Richard E. Smalley Institute for Nanoscale Science and Technology, Rice University, 6100 Main Street, Houston, Texas 77005, United States

[§]Department of Energy Science, Sungkyunkwan University, 300 Cheoncheon-dong, Jangan-gu, Suwon 440-746, Korea

Ⓢ Supporting Information

ABSTRACT: A new method and instrumentation are described for rapid compositional analysis of single-walled carbon nanotube (SWCNT) samples. The customized optical system uses multiple fixed-wavelength lasers to excite NIR fluorescence from SWCNTs individualized in aqueous suspensions. The emission spectra are efficiently captured by a NIR spectrometer with InGaAs multichannel detector and then analyzed by a computer program that consults a database of SWCNT spectral parameters. The identities and relative abundances of semiconducting SWCNTs species are quickly deduced and displayed in graphs and tables. Results are found to be consistent with those based on manual interpretation of full excitation–emission scans from a conventional spectrofluorometer. The new instrument also measures absorption spectra using a broadband lamp and multichannel spectrometers, allowing samples to be automatically characterized by their emission efficiencies. The system provides rapid data acquisition and is sensitive enough to detect the fluorescence of a few picograms of SWCNTs in ∼50 μL sample volumes.
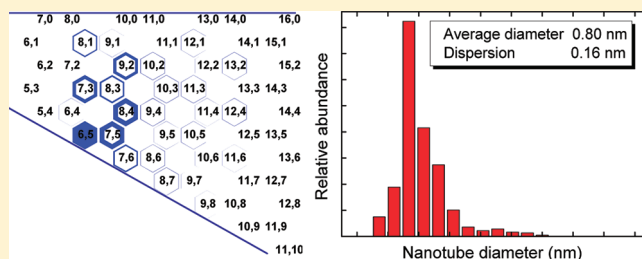
Single-walled carbon nanotubes (SWCNTs) constitute a family of novel nanomaterials of great interest for their unusual physical properties and potential applications. All SWCNTs are ordered tubular arrays of carbon atoms covalently linked by sp^2 bonds. However, they may differ in diameter (d_t), roll-up angle (θ), and length (l). The electronic properties of high aspect ratio SWCNTs are independent of length but vary strongly with diameter and roll-up angle. These two parameters are uniquely defined by a pair of integers (n,m) that index all possible SWCNT structures by reference to a graphene sheet. SWCNTs in which $n-m$ is evenly divisible by 3 are metallic or semimetallic, whereas others are semiconducting.[1] Moreover, the semiconducting band gaps are nearly proportional to inverse diameter and also depend on roll-up angle. A semiconducting SWCNT with diameter near 1 nm has band gap absorption and emission (E_{11}) in the near-IR (NIR). Each such semiconducting nanotube also has visible and near-UV optical transitions (E_{22}, E_{33}, etc.; see Figure 1S, Supporting Information).

Characterization of (n,m) compositions is essential for a variety of SWCNT applications that call for a single or narrow range of structures.[2] Because all currently practical growth methods produce a variety of structures,[3−5] the development of methods for selective growth and effective postgrowth sorting are important tasks that require (n,m) analyses of bulk SWCNT samples. Another important area needing (n,m) analysis is basic research on the structure-dependent chemical reactions and physical processes of SWCNTs.

There are several approaches for estimating SWCNT (n,m) distributions. With microscopic imaging tools such as HRTEM, electron nanodiffraction, STM, and AFM, the strategy is to distinguish the structures of many individual nanotubes and compile the set of "single-particle" results into a distribution. This is generally tedious because many nanotubes must be measured to suppress statistical uncertainties. Systematic sampling errors may also arise if the measured nanotubes do not represent the full sample. These factors and high instrumentation costs make microscopic SWCNT characterization methods unsuitable for routine use.

The dominant bulk analysis methods for SWCNTs are Raman,[6−10] UV−vis-NIR absorption,[11−15] and NIR fluorescence spectroscopies.[3−5,16] Raman analysis exploits the inverse dependence of the radial breathing mode (RBM) frequency on nanotube diameter. RBM spectral analysis can be applied to both semiconducting and metallic SWCNTs, but the Raman signals are strongly dominated by species with electronic transitions in resonance with the incident or scattered photons. This resonance spectral window is narrow compared to the range of electronic transitions present in typical samples, so only the subset of near-resonant (n,m) species are observed in single-laser Raman spectra. This problem can be overcome by measuring
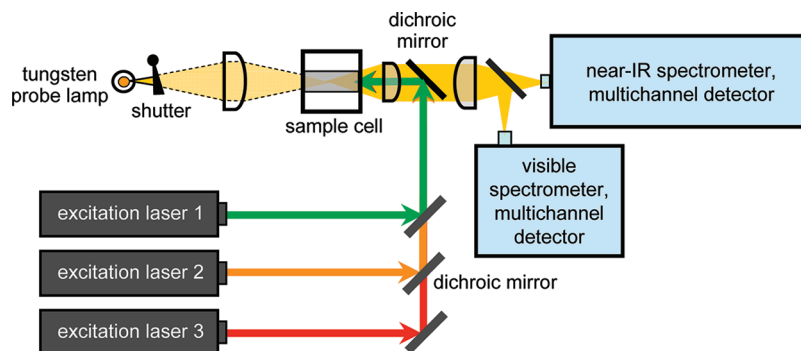
Figure 1. Optical schematic diagram of the nanotube fluorometer. Excitation diode lasers are electrically activated in sequence (with the probe lamp shuttered) to generate three NIR emission spectra. Single-beam absorption spectra are acquired with the lasers switched off and the probe beam shutter raised to allow light from the tungsten lamp to pass through the sample and into the NIR and visible spectrometers.

Raman spectra with many incident wavelengths, but the expense and complexity of multiwavelength Raman spectroscopy limits it to specialized research applications.

Electronic absorption spectroscopy is another characterization method. All semiconducting and metallic (n,m) species show absorption peaks in the NIR and/or visible at wavelengths characteristic of their structures. The required instrumentation is conventional and relatively inexpensive. However, detailed analysis through absorption spectroscopy is hampered by two effects. First, the (n,m) species in a typical mixed SWCNT sample give a dense array of absorption peaks with separations comparable to their widths. This spectral congestion can make analysis problematic even for well dispersed and individualized samples. Modest aggregation broadens the peaks and further blurs the spectral structure. In addition, the distinct (n,m)-specific absorption features appear above a broad, featureless, and often strong background absorption. The detailed sources of this background remain an active research topic;[17] one contribution comes from carbonaceous impurities as considered in the purity analysis method of Itkis et al.[18] Success in deducing (n,m) contents and abundances from SWCNT absorption spectra has been limited by the combined problems of backgrounds and overlapping resonant features.

The newest bulk SWCNT spectroscopy is NIR fluorescence, based on distinct band gap photoluminescence from disaggregated (individualized) SWCNTs.[12] This technique is more sensitive than Raman or absorption and can detect, identify, and quantify SWCNTs at trace concentrations. Fluorescence analysis is possible only for semiconducting species (statistically 2/3 of nanotubes) because metallic species are nonemissive. However, in contrast to absorption methods, there is essentially no NIR fluorescence background to model and subtract. The observed spectrum is also less congested than in absorption because emission is enhanced from the subset of (n,m) species nearly resonant with the excitation wavelength. Fluorescence spectroscopy avoids the "too selective" excitation problems of resonant Raman spectroscopy through higher sensitivity. First, one can often measure SWCNT fluorescence using weak tunable excitation from a simple lamp and monochromator rather than expensive tunable or multiwavelength lasers needed for Raman. Second, the resonant spectral window for fluorescence excitation is broader than for Raman because a species can be detected through excitation of weak sideband and off-resonant absorptions in addition to its main excitation peak. Finally, the wide fluorescence dynamic range, combined with substantial spectral
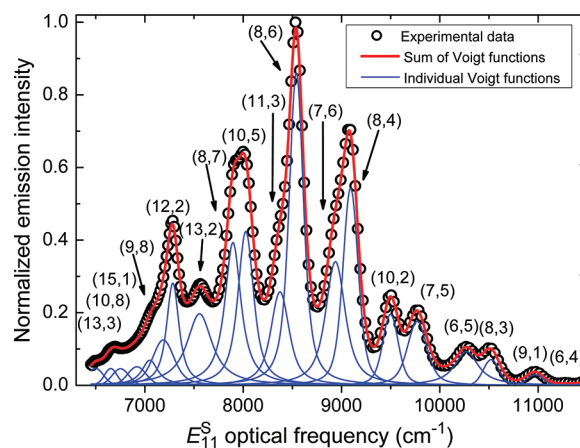
Figure 2. Fluorescence emission from a HiPco SWCNT sample excited at 785 nm. Open circles show experimental data, blue lines show contributions from indicated (n,m) nanotube species, and the red line shows the full simulated emission spectrum.

separations between emission peaks of many (n,m) species, permits minor emitting species to be distinguished from dominant emitters. Fluorescence can therefore be clearly observed from a wide range of (n,m) species using only a few fixed excitation wavelengths.

We describe here a practical realization of this idea: a specialized apparatus and algorithms for efficient fluorimetric SWCNT analysis using a small set of fixed-wavelength diode lasers. Because these lasers are more powerful and focusable than the monochromated lamp of a general purpose spectrofluorometer, our system gives orders of magnitude higher sensitivity. However, it must disentangle the spectral contributions of many (n,m) species based only on a few one-dimensional slices of the full two-dimensional excitation—emission map obtained by a scanning instrument. Our data analysis addresses this problem by combined fitting of the emission spectra under constraints based on prior spectroscopic knowledge about a large set of SWCNT (n,m) species.

■ METHODS

Experimental Section. Two-dimensional fluorescence excitation—emission scans were measured with a Spex Fluorolog 3-211 (J-Y Horiba) spectrofluorometer with a single-channel InGaAs detector. One-dimensional emission spectra (induced by discrete

excitation wavelengths) were acquired using a prototype of the model NS1 NanoSpectralyzer (Applied NanoFluorescence, LLC), an automated nanotube fluorometer system. Figure 1 shows an optical schematic diagram of this instrument. (See Supporting Information for details.)

Spectral and Photophysical Modeling for Data Analysis. When a SWCNT sample containing multiple (n,m) species is excited at a single wavelength, it emits a superposition of peaks from the different species, as illustrated in Figure 2. The spectrum induced by a different excitation wavelength will contain many of the same peaks, but with different intensities reflecting the dependence of excitation efficiencies on the match with (n,m)-specific absorption peaks. We seek to find the sample's relative (n,m) concentrations by analyzing a small number of emission spectra.

For excitation by the ith laser, at frequency ν_{exc}^i, the fluorescence observed from semiconducting species (n,m) in an optically thin sample can be expressed as

$$S_{n,m}^i(\nu_{em})$$
$$= F_{instr}(\nu_{em}) \cdot [C]_{n,m} \cdot P(\nu_{exc}^i) \cdot \sigma_{rel}(\nu_{exc}^i)_{n,m} \cdot f_{n,m}(\nu_{em} - \nu_{n,m}) \cdot (\sigma_{22}\Phi_{Fl})_{n,m} \tag{1}$$

Here, $S_{n,m}^i(\nu_{em})$ is the measured emission signal at optical frequency ν_{em}; $F_{instr}(\nu_{em})$ represents the detection system collection efficiency and response function at that frequency; $[C]_{n,m}$ is the carbon atom concentration from (n,m) SWCNTs; $P(\nu_{exc}^i)$ is the photon irradiance at the sample from the ith excitation beam; each dimensionless relative excitation factor $\sigma_{rel}(\nu_{exc}^i)_{n,m}$ equals $((\sigma(\nu_{exc}^i))/(\sigma_{22}))_{n,m}$, the (n,m)-specific absorption cross section per atom at the excitation wavelength relative to the E_{22} peak cross section; $(\sigma_{22}\Phi_{Fl})_{n,m}$ is the photoluminescence action cross-section (product of peak E_{22} cross section and fluorescence quantum yield) for (n,m) SWCNTs; and $f_{n,m}(\nu_{em} - \nu_{n,m})$ is the area-normalized emission line shape function for (n,m) SWCNTs, centered at $\nu_{n,m}$, their E_{11} peak frequency. The emission spectrum of a mixed sample is a superposition of such individual (n,m) components:

$$S_{total}^i(\nu_{em}) = \sum_{(n,m)} S_{n,m}^i(\nu_{em}) \tag{2}$$

Our spectrofluorimetric analysis goal is to use a small number of spectra, $S_{total}^i(\nu_{em})$, to deduce the relative $[C]_{n,m}$ concentrations. Therefore, the remaining (n,m)-dependent factors in eq 1 must be evaluated, as discussed below.

Detection System Response Function. The instrument's wavelength-dependent optical response was determined using a calibrated irradiance lamp to illuminate the NIR detection optical fiber. We measured InGaAs detector nonlinearity by recording signals as a function of integration time with fixed illumination. Results were fit to obtain a smooth correction function. We measured raw fluorescence spectra on a linear wavelength scale and then corrected for nonlinearity and wavelength dependence before transforming to the optical frequency domain for analysis.

Excitation Profiles. Each excitation factor $\sigma_{rel}(\nu_{exc}^i)_{n,m}$ is the absorption cross section of an (n,m) species at the frequency of the ith excitation laser, relative to its E_{22} peak value. This equals the relative emission intensity for off-resonance versus resonant excitation of that species, assuming that the fluorescence quantum yield is independent of excitation frequency near E_{22}.

Modeling of excitation profiles is currently the most complex and approximate part of our analysis scheme. For each combination of laser frequency and (n,m) species, we compute an empirically based excitation factor using a model developed from spectral studies of mixed and sorted SWCNT samples. In this model, the leading term is the main E_{22} peak, which has a Lorentzian shape in the frequency domain:

$$[\sigma_{rel}(\nu_{exc}^i)_{n,m}]_1 = \cfrac{1}{1 + \left(\cfrac{\nu_{exc}^i - (\nu_{22})_{n,m}}{(\Delta\nu_{22}/2)_{n,m}}\right)^2} \tag{3}$$

Our studies (see Supporting Information Section II and Figure S3) show that the fwhm, $\Delta\nu_{22}$, depends on peak frequency, ν_{22}, according to the empirical relation:

$$\Delta\nu_{22} = A \cdot \exp\left(\frac{-b}{\nu_{22}}\right) \tag{4}$$

with parameters $A = 3590$ cm^{-1} (0.445 eV) and $b = 27\,380$ cm^{-1} (3.395 eV).

In addition to this main E_{22} peak, our model excitation profile (eq 5) includes three terms representing phonon sideband absorptions[19,20] and one frequency-independent background term. On the basis of the features of the (6,4) excitation spectrum shown in Figure S3, Supporting Information, the side bands for all (n,m) species are taken to be Lorentzians centered 1700, 3400, and 5100 cm^{-1} above the main E_{22} peak, with equal widths of twice the main peak width plus 100 cm^{-1}. The shapes of the (n,m)-specific side bands $[\sigma_{rel}(\nu_{exc}^i)_{n,m}]_j$ for $j = 2$ to 4 are computed from equations analogous to eq 3 with appropriately shifted center frequencies. The functions are then multiplied by (n,m)-common amplitude parameters a_j that are adjustable during spectral simulation. Amplitude a_5 represents frequency-independent background absorption, as is present in the excitation spectrum of Figure S3, Supporting Information. Finally, we include a sixth empirically based term representing fluorescence excitation through a short wavelength sideband of the main E_{11} transition. A Lorentzian centered 1600 cm^{-1} above E_{11} with twice the E_{11} width is evaluated at the excitation frequency and multiplied by amplitude factor a_6. This term is irrelevant when the excitation wavelength lies far from E_{11}, but it can be important for smaller diameter SWCNTs excited at longer wavelengths (e.g., (9,1) nanotubes excited at 785 nm). The value of a_6 is therefore held at zero for most (n,m) species but allowed to vary during fitting for long wavelength excitation of those species that are candidates for sideband excitation. The total excitation profile then has the form:

$$\sigma_{rel}(\nu_{exc}^i)_{n,m} = [\sigma_{rel}(\nu_{exc}^i)_{n,m}]_1 + \sum_{j=2}^{4} a_j[\sigma_{rel,j}(\nu_{exc}^i)_{n,m}]_j$$
$$+ a_5 + (a_6^i)_{n,m}\sigma_{rel,6}(\nu_{exc}^i)_{n,m} \tag{5}$$

Emission Line Shape Function. Each excited (n,m) species gives NIR fluorescence represented by the emission line shape function $f_{n,m}(\nu_{em} - \nu_{n,m})$, where the peak frequency $\nu_{n,m}$ is known rather precisely from published spectroscopic studies.[21] Although emission spectra of individual SWCNTs are often nearly Lorentzian,[8,22] those components in bulk samples are better represented as Voigt functions. These Lorentzian/Gaussian

convolutions include a parameter μ that ranges from 0 for a pure Gaussian to 1 for a pure Lorentzian.

To avoid frequent recalculation of the tedious integrals needed to define Voigt line shapes, our simulations use a set of 101 precisely precalculated Voigt functions with μ values spanning the entire range. During fitting, the appropriate Voigt function is retrieved from this set and then scaled in width and offset in frequency to represent an individual (n,m) peak. In numerous simulations of experimental data for SWCNTs dispersed in aqueous SDS or SDBS, we typically find values of fwhm between 150 and 180 cm^{-1} and μ near 0.6 for major emission components. However, simulations are relatively insensitive to these parameter values for minor peaks.

Fluorimetric Efficiencies. The final factor in eq 1, $(\sigma_{22}\Phi_{Fl})_{n,m}$, is the (n,m)-dependent photoluminescence action cross-section. This reflects differences among semiconducting SWCNT species in fluorimetric efficiency or the spectrally integrated fluorescence per carbon atom when equivalently excited at their E_{22} peaks. Relative fluorimetric efficiency factors are challenging to predict by theory, and only a limited number of experimental values have been reported.[23] Available measurements show $(\sigma_{22}\Phi_{Fl})_{n,m}$ variations that exceed a factor of 3,[23] implying the need to include efficiency factors in proper fluorimetric determinations of (n,m) distributions. Nevertheless, because complete information on $(\sigma_{22}\Phi_{Fl})_{n,m}$ values has been unavailable, they are commonly assumed to be equal in fluorimetric data analyses. Further research in SWCNT photophysics should provide the expanded set of empirical $(\sigma_{22}\Phi_{Fl})_{n,m}$ values that are needed to correctly find (n,m) distributions from fluorimetric data and eq 1.

Spectral Data Analysis for Sample Characterization. *Least-Squares Fitting.* The emission spectra obtained with different excitation wavelengths are analyzed together to deduce a sample's (n,m) distribution, $\{[C_{n,m}]\}$. Each experimental spectrum, $S^{i}_{exper}(\nu_{em})$, is compared to a simulated spectrum, $S^{i}_{sim}(\nu_{em})$, computed using eqs 1 and 2. The relative (n,m) concentrations in eq 1 are varied to obtain the best overall match between simulated and experimental spectra, considering all excitation wavelengths, and the optimized set of concentrations is taken as the deduced (n,m) distribution.

We measure relative fit quality from the sum of squared deviations, SSD, between simulated and experimental spectra, including all discrete spectral data points, k, in all spectra, i:

$$\text{SSD} = \sum_{i}\sum_{k}[S^{i}_{sim}(\nu_{em,k}) - S^{i}_{exper}(\nu_{em,k})]^2 \qquad (6)$$

The 900 to 1600 nm spectral range typical of InGaAs detectors can capture fluorescence from $\sim$55 semiconducting (n,m) species. The simulation therefore may include all of these species, or a subset appropriate for the sample, as spectral "basis functions" in eq 2. The SSD value is minimized using a Simplex search algorithm with the constraint of non-negative (n,m) concentrations.[24] eqs 1–6 show that simulated spectra depend not only on $\{[C_{n,m}]\}$ but also on several instrumental and photophysical parameters including relative excitation intensities, spectral peak positions, spectral widths, emission line shape factors, and coefficients in the excitation profile. Most of these can be found or closely estimated from independent experiments. Others, particularly $\{[C_{n,m}]\}$, are deduced by adjustment during SSD minimization. Each type of parameter can independently be selected as fixed or variable during a fitting calculation, and those that vary can be restricted to specified relative changes from their
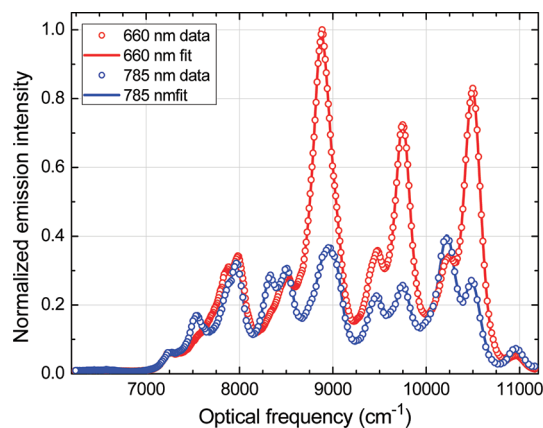
Figure 3. Superimposed experimental and simulated emission spectra (vs frequency) obtained using two excitation lasers and the fitting process described in the text.

starting values. Such constrained variations are useful when analyzing SWCNT samples having transitions slightly shifted or broadened by changes in surfactant, mild aggregation, chemical exposure, etc. Simulations closely matching the measured data, like those shown in Figure 3, require adjustments of $\nu_{n,m}$ peak frequencies to within $\sim$10 cm^{-1} ($\sim$0.1%). As this tolerance is much tighter than the $\sim$2% surfactant-related shifts, it is useful to construct and save spectral templates containing sets of precise spectral parameters appropriate for commonly used surfactants. The typical approach to controlling parameter variations during fitting is outlined in Supporting Information.

Our combined fitting method can be used with any number of excitation wavelengths. As the number of wavelengths increases, the expanded spectral data set improves discrimination between (n,m) species with similar emission peaks and increases redundancy in determining relative concentrations of other species. The dependence of analytical performance on number of excitation wavelengths is discussed in Results and Discussion.

Abundance and Diameter Distributions. Deduced relative (n,m) carbon atom concentrations are converted into fractional abundances, $A_{n,m}$, using the relation

$$A_{n,m} = \frac{[C_{n,m}]}{\sum_{(n,m)}[C_{n,m}]} \qquad (7)$$

These $A_{n,m}$ values are graphically displayed in a graphene sheet plot (see Figure 4 right-hand panels). The thickness of each hexagonal cell border is proportional to the deduced abundance of that (n,m) species.[4] Such graphene sheet plots illustrate how species abundances vary with nanotube diameter and roll-up angle. Diameter distributions are often of special interest. Because each (n,m) species diameter is precisely known from simple geometry,[1] it is straightforward to convert the set of $A_{n,m}$ values into a diameter histogram, as in the Figure 4 left-hand panels. The calculated mean diameter and diameter dispersion (first and second moments) are automatically computed and displayed on the graph.

■ RESULTS AND DISCUSSION

Comparison of 2D and 1D Analyses. The usual approach to fluorimetric SWCNT analysis is based on measurement of full

7434

dx.doi.org/10.1021/ac2014788 |*Anal. Chem.* 2011, 83, 7431–7437
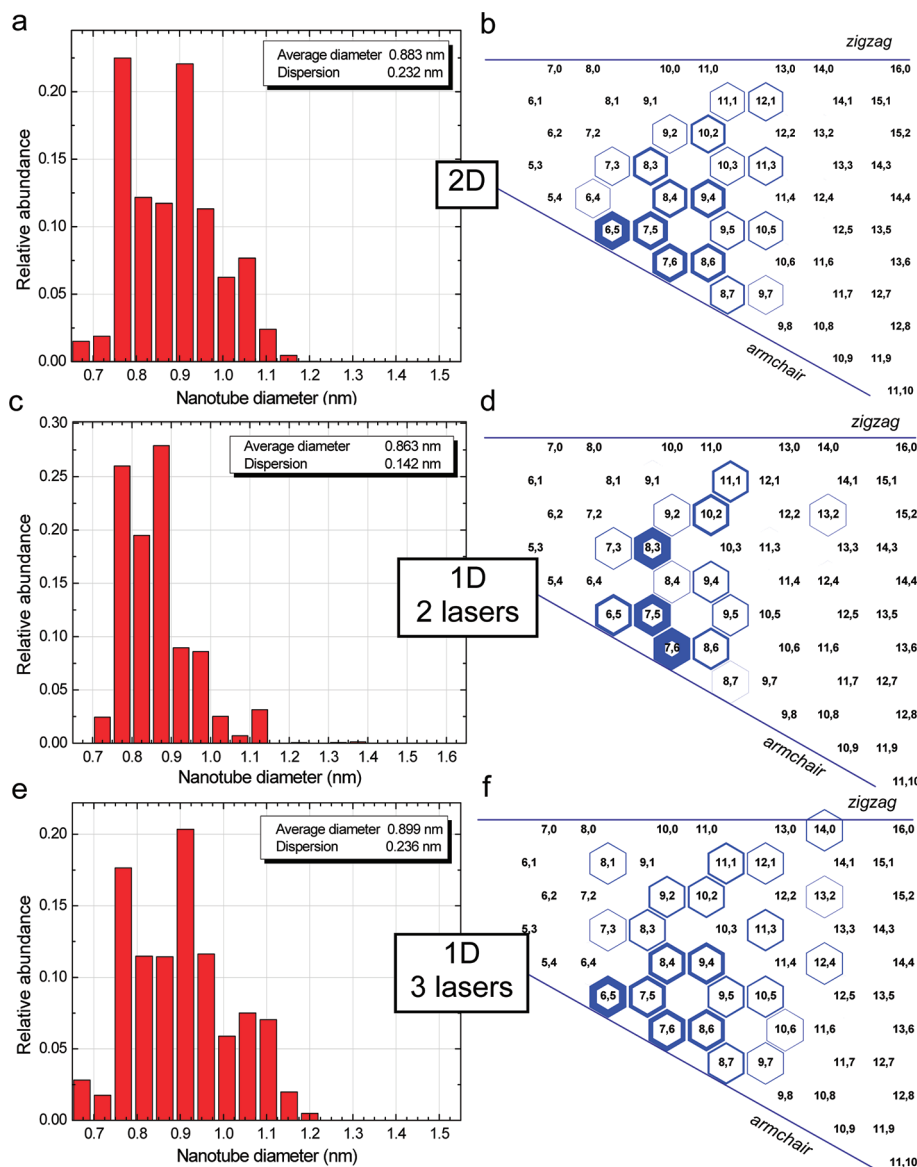
Figure 4. Comparison of distributions determined from 2D data (a,b) versus 1D data using two (c,d) excitation lasers (660 and 785 nm) and three (e,f) excitation lasers (660, 729, and 785 nm). Diameter distribution histograms are shown in a, c, and e; graphene sheet plots representing the calculated (n,m) relative species abundances are shown in b, d, and f.

2D excitation—emission maps,[4] rather than a few excitation slices as described here. Although our few-slice method greatly increases data collection speed and sensitivity, it is necessary to compare its analytical findings with those of the 2D approach.

For this comparison, a stable dispersion of HiPco SWCNTs was prepared and fluorimetrically analyzed using both methods. The 2D map data were corrected for wavelength-dependent excitation intensity and detection sensitivity and transformed into optical frequency. The signal from each (n,m) species was then found by integrating its peak along the emission axis at the excitation frequency giving maximum emission. We assumed constant fluorescence efficiency factors $(\sigma_{22}\Phi_{Fl})_{n,m}$ in both analyses. Figure 4 shows the deduced diameter and (n,m) distributions from the 2D analysis in the top frames, from the 1D analysis with two excitation wavelengths in the middle, and from the 1D analysis with three excitation wavelengths in the bottom. The three distributions are qualitatively similar, and differences are

particularly minor between the three-laser and 2D analyses. Average diameters found from the 1D analyses agree with the 2D result to within 2%. The time needed to acquire the 2D data set exceeded 20 h, whereas the 1D data sets were acquired in seconds. Even if the 2D acquisition time were reduced by substituting a multichannel InGaAs array for the single channel detector, our laser-based instrument would still provide much quicker fluorimetric analysis.

Analysis Accuracy versus Number of Excitation Wavelengths. As the few-slice 1D approach is extended to include more excitation wavelengths, it should converge to the 2D analysis. To check, we extracted various 1D slices from a full 2D data set and analyzed them using the fitting procedure described above. We tested several combinations of two and three excitation wavelengths as well as single sets of four, five, and seven excitation wavelengths. The selected wavelengths were close to standard laser sources that might be used in an enhanced
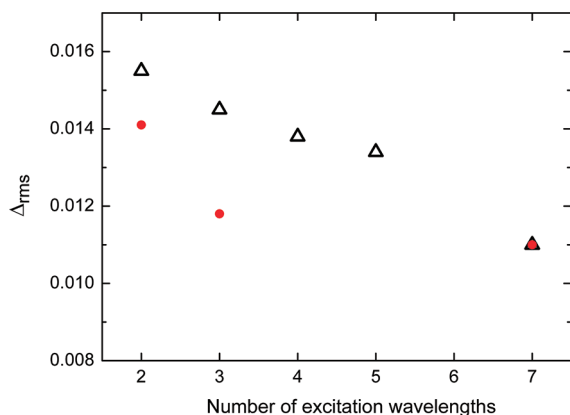
Figure 5. Root-mean-square deviations of relative abundances deduced from 1D data sets with different numbers of excitation wavelengths, as compared to abundances deduced from 2D data. Open triangles mark analyses from data sets containing 639 and 681 nm excitation wavelengths; solid circles mark analyses containing 660 and 785 wavelengths.

laser-based instrument. The analysis from each excitation set was compared with the full 2D analysis by computing the root-mean-square difference between deduced relative abundances, including all N of the (n,m) basis species required for the simulation:

$$\Delta_{\mathrm{rms}} = \sqrt{\frac{\sum_{(n,m)} \left[A_{(n,m)}^{1D} - A_{(n,m)}^{2D} \right]^2}{N}} \qquad (8)$$

As plotted in Figure 5 and listed in Table S3, Supporting Information, the Δ_{rms} values varied between 0.011 and 0.017 and monotonically decreased with increasing numbers of discrete excitation wavelengths. This slow convergence to the 2D results can be accelerated by choosing a set of specific 1D wavelengths that properly span the range of E_{22} resonances in a sample. The use of our analysis method with only a few excitation wavelengths typically provides fractional abundance results matching the 2D values within approximately 1 to 2% for samples containing a wide range of species.

Sample Quality Assessment. SWCNT suspensions vary in their contents of aggregated SWCNTs, structurally defective SWCNTs, chemically functionalized SWCNTs, double- or multiwalled CNTs, amorphous carbon, residual catalyst, and giant fullerenes. All of these "impurities" can absorb light at typical E_{22} transition wavelengths, but structured NIR emission arises only from disaggregated SWCNTs largely free of defects and sidewall functionalization. Generally, a sample's overall NIR fluorescence efficiency will therefore be greatest when it contains only pristine, individually suspended SWCNTs. We propose that bulk fluorescence efficiency, as a ratio of emission to absorption, should be used as an index of sample purity and quality.

A simple measure of fluorescence efficiency is the ratio of spectrally integrated fluorescence emission to absorbance at the excitation wavelength. Provided that the sample is optically thin (absorbance below ∼0.1) through the limited active depth (∼1 mm), this gives a simple "quality index" that allows comparison of disaggregation and purity among samples with similar (n,m) distributions. Although absolute values of this index depend on instrument-specific factors, relative values measured within a laboratory are very useful for comparing and optimizing SWCNT sample preparation methods. This quality index is
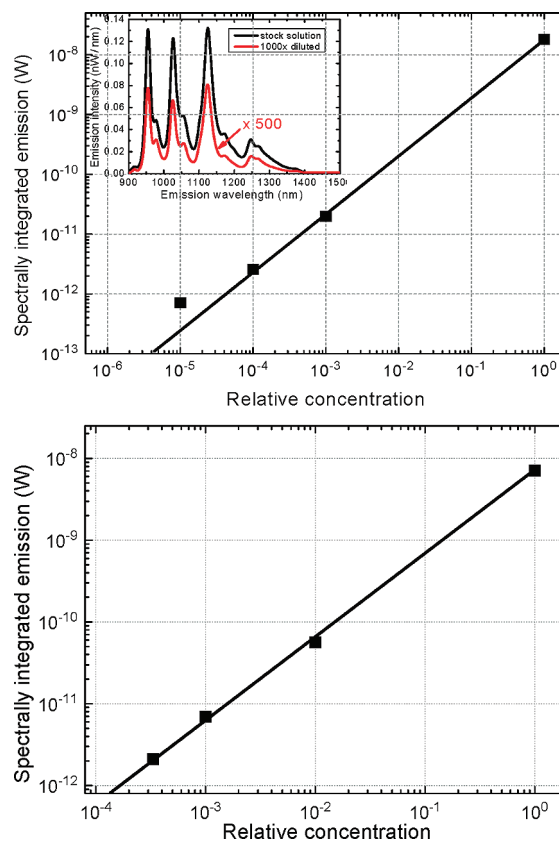
Figure 6. Spectrally integrated fluorescence intensity vs sample concentration for SWCNTs in SDBS/H_2O (top frame) and PFO/toluene (bottom frame). Inset in top frame shows emission spectra of SDBS/H_2O stock solution before and after 1000-fold dilution.

automatically computed using the system shown in Figure 1, which measures both fluorescence and absorption spectra under program control. We find that quality indices can vary by several orders of magnitude among dispersed SWCNT samples.

SWCNT Trace Detection and Sensitivity Limits. To test the sensitivity of our laser-based nanotube fluorometer, we prepared stock solutions of HiPco SWCNTs in SDBS/H_2O and PFO/toluene and recorded full emission and absorption spectra. Their concentrations were estimated from absorbance at 763 nm using the mass absorptivity value of 0.043 L mg^{-1} cm^{-1}.[25] The stock samples were then diluted by factors of 10^3, 10^4, and 10^5 using aqueous SDBS or toluene, and the diluted samples were bath sonicated for ∼5 min. We measured emission spectra from ∼45 μL volumes of each diluted sample using relatively long total integration times of 17.5 s (SDBS) or 1.5 s (PFO). The accumulated signals were automatically divided by integration time.

Figure 6 shows the spectrally integrated fluorescence signals as a function of dilution. Emission spectra of the SDBS stock solution before and after 1000-fold dilution are plotted in the top frame inset, with the diluted spectrum scaled up by a factor of 500 for clarity. The aqueous SWCNT concentrations ranged from approximately 18 mg/L (stock) to 150 ng/L at the greatest plotted dilution, where the sample volume contained ∼8 pg (∼200 ppt) of SWCNTs. Although the concentration of the PFO/toluene stock sample was approximately 10 times lower than that of the SDBS/H_2O stock, its integrated emission remained linear over a dilution range of at least 3000, to concentrations below 500 ng/L.

We expect that modest refinements in sample handling and data acquisition will permit bulk fluorimetric analysis of SWCNTs in many liquid samples at the subpicogram level, corresponding to mass fractions approaching 1 part in 10^{11}.

CONCLUSIONS

We describe a practical emission and absorption spectrometer designed to detect, identify, and quantify numerous SWCNT structural species in typical bulk samples. The system uses a customized optical configuration with fixed-wavelength diode lasers to excite emission, a broadband lamp to probe absorption spectra, and NIR and visible multichannel spectrometers for absorption and fluorescence measurements. NIR fluorescence spectra show several slices of a full 2D excitation—emission scan. These are interpreted by a specialized, integrated data simulation/analysis program that consults a database of SWCNT spectral parameters to deduce detailed compositional results and present them as tables and graphs. SWCNT sample quality is automatically assessed by normalizing the fluorescence intensity to sample absorbance. As compared to conventional 2D excitation—emission scans using monochromated lamp excitation, our approach enhances sensitivity or data acquisition speed by 3 to 4 orders of magnitude because it uses powerful, focusable excitation lasers and high aperture collection optics. The system can detect a few picograms of SWCNTs in liquid media, at mass fractions of $\sim 10^{-10}$.

The main challenge in our method is deducing SWCNT compositions from discrete slices of the full excitation—emission surface. This is currently achieved using empirically based models for SWCNT excitation and emission spectra. Approximations in these models can lead to analysis inaccuracies, which should diminish as future research on structurally sorted samples allows refinement of the spectral models. Another source of uncertainty is clusters of overlapping emission peaks from several (n,m) species. If the number of excitation wavelengths is smaller than the number of species represented in a cluster, there will be ambiguities in determining their concentrations. As can be inferred from Figure S6, Supporting Information, such clusters of peaks below 1600 nm may include up to five (n,m) species. The use of four or five excitation wavelengths (a very feasible configuration) will generally allow analyses that are comparable to those obtained from full excitation—emission scans.

ASSOCIATED CONTENT

S **Supporting Information.** Information describing instrumentation and experimental details; data used to deduce E_{22} line widths and excitation profiles; and tables with typical spectral parameters. This material is available free of charge via the Internet at http://pubs.acs.org.

AUTHOR INFORMATION

Corresponding Author
*E-mail: weisman@rice.edu.

Present Addresses
‡SouthWest NanoTechnologies, Inc., 2501 Technology Place, Norman, OK 73071, United States.

ACKNOWLEDGMENT

REFERENCES

(1) Saito, R.; Dresselhaus, G.; Dresselhaus, M. S. *Physical Properties of Carbon Nanotubes*; Imperial College Press: London, 1998.

(2) Arepalli, S.; Nikolaev, P.; Gorelik, O. Analytical Characterization of Single Wall Carbon Nanotubes. In *Encyclopedia of Nanoscience and Nanotechnology*; American Scientific Publishers: Stevenson Ranch, CA, 2004; Vol. 1, pp 51—67.

(3) Bachilo, S. M.; Strano, M. S.; Kittrell, C.; Hauge, R. H.; Smalley, R. E.; Weisman, R. B. *Science* 2002, 298, 2361–2366.

(4) Bachilo, S. M.; Balzano, L.; Herrera, J. E.; Pompeo, F.; Resasco, D. E.; Weisman, R. B. *J. Am. Chem. Soc.* 2003, 125, 11186–11187.

(5) Lebedkin, S.; Hennrich, F. H.; Skipa, T.; Kappes, M. M. *J. Phys. Chem. B* 2003, 107, 1949–1956.

(6) Rao, A. M.; Richter, E.; Bandow, S.; Chase, B.; Eklund, P. C.; Williams, K. A.; Fang, S. L.; Subbaswamy, K. R.; Menon, M.; Thess, A.; Smalley, R. E.; Dresselhaus, G.; Dresselhaus, M. S. *Science* 1997, 275, 187–191.

(7) Kataura, H.; Kumazawa, Y.; Maniwa, Y.; Umezu, I.; Suzuki, S.; Ohtsuka, Y.; Achiba, Y. *Synth. Met.* 1999, 103, 2555–2558.

(8) Hartschuh, A.; Pedrosa, H. N.; Novotny, L.; Krauss, T. D. *Science* 2003, 301, 1354–1356.

(9) Dresselhaus, M. S.; Dresselhaus, G.; Jorio, A.; Souza Filho, A. G.; Pimenta, M. A.; Saito, R. *Acc. Chem. Res.* 2002, 35, 1070–1078.

(10) Strano, M. S.; Doorn, S. K.; Haroz, E. K.; Kittrell, C.; Hauge, R. H.; Smalley, R. E. *Nano Lett.* 2003, 3, 1091–1096.

(11) Kazaoui, S.; Minami, N.; Yamawaki, H.; Aoki, K.; Kataura, H.; Achiba, Y. *Phys. Rev. B* 2000, 62, 1643–1646.

(12) O'Connell, M. J.; Bachilo, S. M.; Huffman, C. B.; Moore, V.; Strano, M. S.; Haroz, E.; Rialon, K.; Boul, P. J.; Noon, W. H.; Kittrell, C.; Ma, J.; Hauge, R. H.; Weisman, R. B.; Smalley, R. E. *Science* 2002, 297, 593–596.

(13) Hagen, A.; Hertel, T. *Nano Lett.* 2003, 3, 383–388.

(14) Lian, Y. F.; Maeda, Y.; Wakahara, T.; Akasaka, T.; Kazaoui, S.; Minami, N.; Choi, N.; Tokumoto, H. *J. Phys. Chem. B* 2003, 107, 12082–12087.

(15) Nair, N.; Usrey, M. L.; Kim, W.; Braatz, R. D.; Strano, M. S. *Anal. Chem.* 2006, 78, 7689–7696.

(16) Lefebvre, J.; Homma, Y.; Finnie, P. *Phys. Rev. Lett.* 2003, 90, 217401—1–217401—4.

(17) Naumov, A. V.; Ghosh, S.; Tsyboulski, D. A.; Bachilo, S. M.; Weisman, R. B. *ACS Nano* 2011, 5, 1639–1648.

(18) Itkis, M. E.; Perea, D. E.; Niyogi, S.; Rickard, S. M.; Hamon, M. A.; Zhao, B.; Haddon, R. C. *Nano Lett.* 2003, 3, 309–314.

(19) Miyauchi, Y.; Maruyama, S. *Phys. Rev. B* 2006, 74, 035415—1–035415/7.

(20) Lefebvre, J.; Finnie, P. *Phys. Rev. Lett.* 2007, 98, 167406—1–167406—4.

(21) Weisman, R. B.; Bachilo, S. M. *Nano Lett.* 2003, 3, 1235–1238.

(22) Tsyboulski, D. A.; Bachilo, S. M.; Weisman, R. B. *Nano Lett.* 2005, 5, 975–979.

(23) Tsyboulski, D.; Rocha, J.-D. R.; Bachilo, S. M.; Cognet, L.; Weisman, R. B. *Nano Lett.* 2007, 7, 3080–3085.

(24) Lawson, C. L.; Hanson, R. J. *Solving Least Square Problems*; Society for Industrial & Applied Mathematics: Philadelphia, 1995.

(25) Moore, V. C. Ph.D. Thesis, Rice University, Houston, TX, 2005.